University of Wollongong

Research Online

Faculty of Engineering and Information Sciences - Papers: Part A

Faculty of Engineering and Information Sciences

1-1-2015

A Fe/Fe3O4/N-carbon composite with hierarchical porous structure and in situ formed N-doped graphene-like layers for high-performance lithium ion batteries

Yao Li
Shanghai Jiao Tong University

Qing Meng
University of Wollongong, qm982@uowmail.edu.au

Shenmin Zhu
Shanghai Jiao Tong University

Zeng-Hui Sun
Shanghai Jiao Tong University

Hao Yang
Shanghai Jiao Tong University

See next page for additional authors

Follow this and additional works at: https://ro.uow.edu.au/eispapers

 Part of the Engineering Commons, and the Science and Technology Studies Commons

Research Online is the open access institutional repository for the University of Wollongong. For further information contact the UOW Library: research-pubs@uow.edu.au

A Fe/Fe3O4/N-carbon composite with hierarchical porous structure and in situ formed N-doped graphene-like layers for high-performance lithium ion batteries

Abstract

Fe/Fe3O4/N-carbon composite consisting of a porous carbon matrix containing a highly conductive N-doped graphene-like network and Fe/Fe3O4 nanoparticles was prepared. The porous carbon has a hierarchical structure which is inherited from rice husk and the N-doped graphene-like network formed in situ. When used as an anode material for lithium batteries, the composite delivered a reversible capacity of approximately 610 mA h g(-1) at a current density of 200 mA g(-1) even after 100 cycles, due to the synergism between the unique hierarchical porous structures, highly electrically conductive N-doped graphene- like networks and nanosized particles of Fe/Fe3O4. This work provides a simple approach to prepare N-doped porous carbon activated nanoparticle composites which could be used to improve the electrochemical performance of lithium ion batteries.

Keywords

formed, situ, structure, porous, hierarchical, composite, carbon, n, fe3o4, fe, lithium, performance, high, batteries, layers, ion, like, graphene, doped

Disciplines

Engineering | Science and Technology Studies

Publication Details

Li, Y., Meng, Q., Zhu, S., Sun, Z., Yang, H., Chen, Z., Zhu, C., Guo, Z. & Zhang, D. (2015). A Fe/Fe3O4/N-carbon composite with hierarchical porous structure and in situ formed N-doped graphene-like layers for high-performance lithium ion batteries. Dalton Transactions: an international journal of inorganic chemistry, 44 (10), 4594-4600.

Authors

Yao Li, Qing Meng, Shenmin Zhu, Zeng-Hui Sun, Hao Yang, Zhixin Chen, Chengling Zhu, Zaiping Guo, and Di Zhang

This journal article is available at Research Online: https://ro.uow.edu.au/eispapers/3929

Dalton Transactions

PAPER

View Article Online
View Journal | View Issue

Published on 09 January 2015. Downloaded by University of Wollongong on 28/04/2015 02:46:58.

Cite this: *Dalton Trans.*, 2015, **44**, 4594

A Fe/Fe_3O_4/N-carbon composite with hierarchical porous structure and *in situ* formed N-doped graphene-like layers for high-performance lithium ion batteries†

Yao Li,[a] Qing Meng,[b] Shen-min Zhu,*[a] Zeng-hui Sun,[a] Hao Yang,[a] Zhi-xin Chen,[b] Cheng-ling Zhu,[a] Zai-ping Guo[b] and Di Zhang*[a]

Received 25th November 2014,
Accepted 7th January 2015

DOI: 10.1039/c4dt03615h

www.rsc.org/dalton

A Fe/Fe_3O_4/N-carbon composite consisting of a porous carbon matrix containing a highly conductive N-doped graphene-like network and Fe/Fe_3O_4 nanoparticles was prepared. The porous carbon has a hierarchical structure which is inherited from rice husk and the N-doped graphene-like network formed *in situ*. When used as an anode material for lithium batteries, the composite delivered a reversible capacity of approximately 610 mA h g^{-1} at a current density of 200 mA g^{-1} even after 100 cycles, due to the synergism between the unique hierarchical porous structures, highly electrically conductive N-doped graphene-like networks and nanosized particles of Fe/Fe_3O_4. This work provides a simple approach to prepare N-doped porous carbon activated nanoparticle composites which could be used to improve the electrochemical performance of lithium ion batteries.

1. Introduction

Lithium ion batteries (LIBs) have been extensively used in portable electronic devices as well as electric vehicles, because of their high energy density, long cycle life, low self-discharge and no "memory effect".[1–4] As an essential part of LIBs, anode materials play an important role in the performance of LIBs and thus attract considerable attention. Accordingly, a variety of new anode materials, such as carbon materials, metal alloys, metal oxides, have been developed.[5–7] Among them, iron oxide is considered as an ideal anode material due to its adequate theoretical capacity (1004 mA h g^{-1} for α-Fe_2O_3 and 924 mA h g^{-1} for Fe_3O_4), low toxicity, and moderate volume change during lithium extraction and insertion processes. However, iron oxide breaks into small metal clusters that can react with Li to form Li_2O, which along with great volume expansion and destruction of the structure upon electrochemical cycling, especially at high rates, results in severe loss of capacity with cycling and a poor electronic conductivity.

Both nanostructure design and composites with porous carbon are useful strategies to improve the reversible capacity and rate capacity. Nanostructures can shorten Li ion insertion/extraction pathways. Composites with porous carbon may buffer volume expansion upon lithium extraction and insertion. Unfortunately, porous carbons involved in the formation of composites are usually amorphous.[8–10] Their low electronic conductivity has to be considered seriously, especially in the LIB system.[11] In order to improve the electronic conductivity, attempts such as introducing graphene-like structures in porous carbon have been made. A graphitized mesoporous carbon produced by CVD has shown a high capacity of about 340 mA h g^{-1} at a rate of 0.1 C.[12] The capacity of ~250 mA h g^{-1} was retained after ten cycles. Similarly, a simple catalysis method was developed for the synthesis of Fe_2O_3/graphitized mesoporous carbon composites, which showed a decent capacity of approximately 623 mA h g^{-1} as well as cycling stability.[13] In addition, nitrogen doping is proved to be another effective way to enhance the electrochemical properties of carbon composites.[14–17] Nitrogen-doped carbonaceous materials may offer more active sites and enhance the interaction between carbon and lithium and thus improve the kinetics of lithium diffusion and transfer.[17] Nitrogen-doped graphene reported in the literature showed an energy density of approximately 199 mA h g^{-1} even at a high current density

[a]State Key Laboratory of Metal Matrix Composites, Shanghai Jiao Tong University, Shanghai 200240, China. E-mail: smzhu@sjtu.edu.cn; Fax: +86 21 3420 2749; Tel: +86 21 3420 2584

[b]The Faculty of Engineering and Information Science, University of Wollongong, NSW 2522, Australia

† Electronic supplementary information (ESI) available: Raman spectra, TGA and galvanostatic charge–discharge curves of RHC, Fe/Fe_3O_4/carbon and Fe/Fe_3O_4/N-carbon and TEM images of Fe/Fe_3O_4/N-carbon composites after 100 discharge/charge cycles. See DOI: 10.1039/c4dt03615h

This journal is © The Royal Society of Chemistry 2015

Published on 09 January 2015. Downloaded by University of Wollongong on 28/04/2015 02:46:58.

of 25 A g^{-1}.[18] The incorporation of a carbon material with a porous structure, graphene-like layers, and nitrogen doping are proposed as feasible ways to improve the electrochemical performance of iron oxides for high performance LIBs.

In this paper, Fe/Fe_3O_4 nanoparticles were embedded into nitrogen doped porous carbon through simple impregnation followed by polymerization and calcination, generating a novel Fe/Fe_3O_4/carbon composite (Fe/Fe_3O_4/N-carbon). The composite is composed of Fe/Fe_3O_4 nanoparticles and porous carbon with a N-doped graphene-like structure. Owing to the high specific capacity of Fe_3O_4, effective buffering provided by the nanostructure and porous carbon composition and the improved electrical conductivity of the electrode by the incorporation of Fe nanoparticles and N-doped graphene-like structures, this Fe/Fe_3O_4/N-carbon showed an enhanced specific capacity and cycling stability.

2. Experimental

2.1. Preparation

Typically, a rice husk precursor was used to fabricate porous carbon (RHC) *via* carbonization at 650 °C, followed by activation at 800 °C with KOH. Then, the calcined RHC was washed with 12% HCl and distilled water. The washed RHC (0.5 g) was mixed with a 1 mL 0.9 M iron chloride ($FeCl_3$) solution. The mixture was exposed to pyrrole vapor at 50 °C for 3 hours, followed by calcination at 850 °C for 2 hours under nitrogen. The product is denoted as Fe/Fe_3O_4/N-carbon. For comparison, the mixture of RHC and iron chloride was treated by the same procedure but without pyrrole vapor exposure. The product fabricated is denoted as Fe/Fe_3O_4/carbon. Pure iron chloride treated by the same procedure is denoted as Fe/Fe_3O_4/N.

2.2. Characterization

Fourier transform-infrared measurements (FT-IR) were conducted on KBr pellets with a PE Paragon 1000 spectrophotometer. The synthesized samples were characterized by X-ray diffraction (XRD) on a RigakuD/max 2550VL/PC system operated at 35 kV and 200 mA with Cu Kα radiation (λ = 1.5406 Å), at a scan rate of 5° min^{-1} and a step size of 0.02°. Raman spectroscopy was measured on a Renishawin Via Raman microscope. X-ray photoelectron spectra (XPS) were collected on a physical electronics PHI5400 using Mg K radiation as the X-ray source. All the spectra were corrected with the C 1s (285.0 eV) band. Elemental analysis was processed using a Vario ELIII/Isoprime isotope ratio mass spectrometer. Nitrogen adsorption measurements at 77 K were performed using an ASAP2020 volumetric adsorption analyzer, after the samples had been outgassed for 8 h in the degas port of the adsorption apparatus. Scanning electron microscopy (SEM) was performed on a JEOL JSM-6360LV field emission microscope at 15 kV. Transmission electron microscopy (TEM) was carried out on a JEOL 2010 microscope at 200 kV. Thermogravimetric analysis (TGA) was conducted on a PE TGA-7 instrument at 20 °C min^{-1}.

2.3. Electrochemical measurements

Electrochemical experiments were carried out in two-electrode Swagelok cells. The working electrodes were made by mixing the Fe/Fe_3O_4/N-carbon composite with carbon black and the binder (polyvinylidene fluoride, PVDF) at a mass ratio of 80 : 10 : 10. The mixture was then spread uniformly onto a copper foil cylinder with a diameter of 12 mm and dried in a vacuum at 80 °C. The net mass loading of the activated material for each tested electrode was between 1.0 and 1.5 mg. The cells were assembled in an argon filled glove box (Mikrouna 1220/750). Metallic lithium foil was used as the counter electrode. The electrolyte was made of 1 M $LiPF_6$ dissolved in a mixture of ethylene carbonate (EC) and diethylene carbonate (DEC) with the volume ratio of 1 : 1. The charge/discharge profiles of the electrodes were collected at room temperature on a Land CT2001A battery test system. The cyclic voltammetry (CV) curves were obtained on a Chenhua CHI 660D electrochemical workstation in the potential range of 0.05–3.0 V at a scan rate of 0.5 mV s^{-1}. Electrochemical impedance spectra were recorded by using a Chenhua CHI 660D electrochemical workstation with an AC voltage signal of 5 mV, in the frequency range between 100 kHz and 5 mHz. For comparison, the electrochemical performances of Fe/Fe_3O_4/carbon were evaluated under the same conditions. The cells were disassembled in the glovebox after 100 cycles, and the working electrode was taken out and washed three times using a dimethyl carbonate (DMC) solution. It was then prepared for TEM observation.

3. Results and discussion

In this work, a Fe/Fe_3O_4/N-carbon composite was synthesized by a three-step method as described in Scheme 1. Firstly, porous carbon fabricated from rice husk (RHC) was pretreated with nitric acid and carboxyl RHC was obtained. Then, the carboxyl RHC was impregnated in a $FeCl_3$ solution, and set in a pyrrole vapour environment at 50 °C for 3 h, during which pyrrole migrated into the pores of carboxyl RHC and *in situ* polymerization of pyrrole occurred due to the catalytic effect of

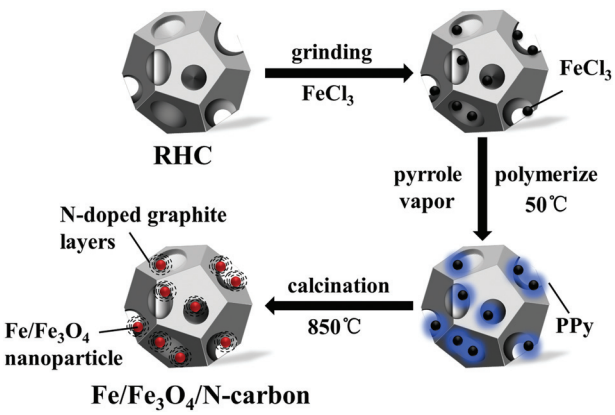

Scheme 1 Schematic illustration of the formation of the Fe/Fe_3O_4/N-carbon composite.

Published on 09 January 2015. Downloaded by University of Wollongong on 28/04/2015 02:46:58.

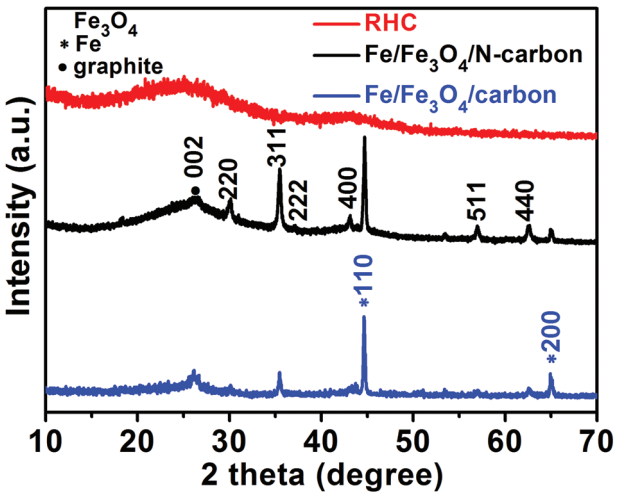

Fig. 1 XRD patterns of RHC, Fe/Fe_3O_4/N-carbon and Fe/Fe_3O_4/carbon.

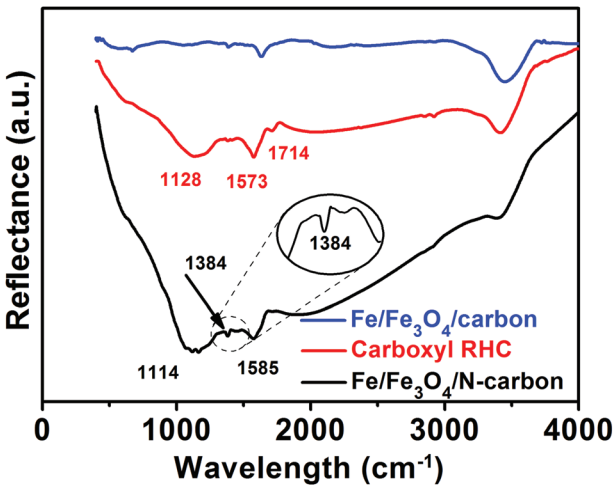

Fig. 2 FTIR spectra of Fe/Fe_3O_4/carbon, carboxyl RHC and Fe/Fe_3O_4/N-carbon.

the impregnated Fe^{3+}. Finally, calcination was performed at 850 °C for 2 h, and during this process the polypyrrole may convert into nitrogen doped graphite layers with iron oxide nanoparticles inside.

Fig. 1 shows XRD patterns of RHC, Fe/Fe_3O_4/carbon and Fe/Fe_3O_4/N-carbon. There is a detectable diffraction peak at 26.4° in the XRD pattern of Fe/Fe_3O_4/N-carbon (Fig. 1), corresponding to an interlayer *d* spacing of approximately 0.34 nm. It indicates the existence of turbostratic ordering of graphene-like materials, similar to those observed in bulk carbon nitride materials.[19] The diffraction peaks at 30.1°, 35.4°, 43.1°, 56.9° and 62.5° can be indexed as (220), (311), (400), (511) and (440) of face-centered cubic Fe_3O_4 (JCPDS no. 19-0629), respectively. The diffraction peaks at 44.7° and 65.0° are indexed as (110) and (200) of body-centered cubic Fe, respectively (JCPDS no. 06-0696). The reduction by carbon of Fe^{3+} species attached on the surface of RHC at a high temperature of 850 °C generates the body-centered cubic Fe. Using the Scherrer formula from the width of the diffraction peak at 35.4°, the average size of Fe_3O_4 particles was estimated to be approximately 45 nm. The XRD pattern of Fe/Fe_3O_4/carbon is similar to that of Fe/Fe_3O_4/N-carbon, thus Fe and Fe_3O_4 particles are also present in Fe/Fe_3O_4/carbon.

The presence of nitrogen in the Fe/Fe_3O_4/N-carbon composite was investigated by using FT-IR (Fig. 2). The FT-IR spectrum of carboxyl RHC shows absorption at 1714 cm^{-1} which is characteristic of C=O stretching vibration, owing to the existence of COOH and absorption at 1573 cm^{-1} which is attributed to asymmetric –COO– stretching.[20] After calcination, the peak from COOH groups disappeared as evidenced by the spectra of both Fe/Fe_3O_4/N-carbon and Fe/Fe_3O_4/carbon. As compared with Fe/Fe_3O_4/carbon, Fe/Fe_3O_4/N-carbon has two new absorptions: (i) at 1585 cm^{-1}, attributed to N–H in-plane deformation vibrations or C=C stretching vibration, and (ii) at 1384 cm^{-1} which is caused by the presence of C–N stretching vibration in the Fe/Fe_3O_4/N-carbon composite.[21] These two extra absorption peaks clearly suggested the presence of nitrogen in Fe/Fe_3O_4/N-carbon.

Raman spectra of RHC, Fe/Fe_3O_4/carbon and Fe/Fe_3O_4/N-carbon are shown in Fig. S1†. Two bands at around 1590 and 1336 cm^{-1} are known as the graphite sp^2 (E_{2g}) carbon band or G band and the defect sp^3 carbon band or D band, respectively.[22,23] For RHC, the D band is significantly higher than the G band: $I_D/I_G > 1$, indicating the high content of the amorphous carbon. The I_D/I_G decreased significantly in Fe/Fe_3O_4/carbon and Fe/Fe_3O_4/N-carbon samples in comparison with that of RHC, indicating the graphitization in both Fe/Fe_3O_4/carbon and Fe/Fe_3O_4/N-carbon samples.[24–27] It should be noted that no band shift was detected for Fe/Fe_3O_4/carbon in comparison with RHC. However, a distinct G band p-shift of 12 cm^{-1} was observed for the sample of Fe/Fe_3O_4/N-carbon, which could be explained by the N-doping of the composite, as reported by others.[27]

The composition of Fe/Fe_3O_4/N-carbon was further investigated by XPS measurements. As expected, all the peaks present in the spectrum (Fig. 3a) can be assigned to carbon (C 1s), nitrogen (N 1s), iron (Fe $2p^3$) and oxygen (O 1s). There are two binding energy peaks in the N 1s pattern (Fig. 3b). The peak at 397.8 eV is assigned to sp^2 hybridized N atoms bonded to

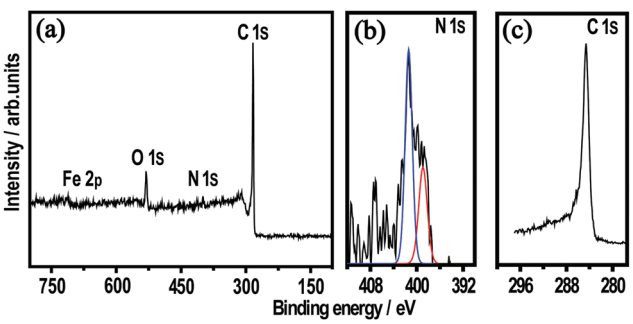

Fig. 3 XPS spectra of Fe/Fe_3O_4/N-carbon.

This journal is © The Royal Society of Chemistry 2015

Published on 09 January 2015. Downloaded by University of Wollongong on 28/04/2015 02:46:58.

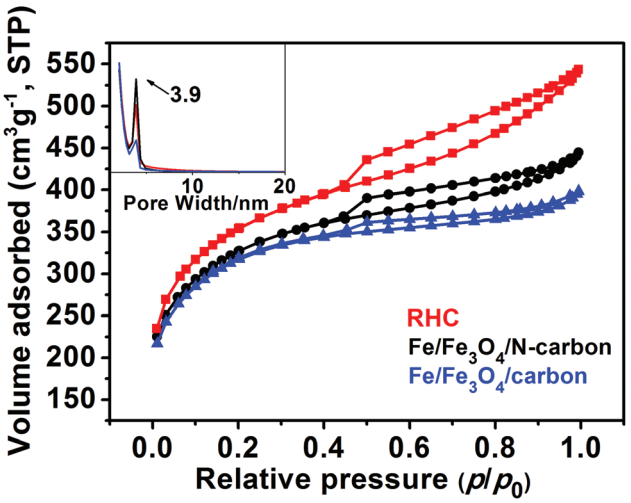

Fig. 4 N_2 adsorption isotherms of RHC, Fe/Fe_3O_4/carbon and Fe/Fe_3O_4/N-carbon.

carbon atoms, and that at 400.2 eV corresponds to pyrrolic N atoms trigonally bonded with sp^2 or sp^3 hybridized carbon atoms.[28] The XPS analyses confirm the existence of pyrrolic nitrogen in the porous composite and are consistent with the C 1s spectrum (Fig. 3c).

Nitrogen adsorption/desorption was conducted to characterize the porous structures (Fig. 4). The specific surface areas of the RHC matrix and Fe/Fe_3O_4/carbon are approximately 1245 and 1116 $m^2\ g^{-1}$, respectively, suggesting that the impregnation and calcination have little effect on the surface area. More interestingly the resulting Fe/Fe_3O_4/N-carbon still has a surface area of 1151 $m^2\ g^{-1}$ (Fig. 4), indicating that the existence of pyrrole vapor did not influence the porous structures. All the samples show a hysteresis loop in the P/P_0 range of 0.45–1.0, and the pore width was around 3.9 nm. The results clearly suggest that the large specific surface area and hierarchical microstructures of RHC were retained in Fe/Fe_3O_4/N-carbon and Fe/Fe_3O_4/carbon. These hierarchical structures would provide a buffering room for volume change and necessarily accessible channels for charge transfer during charge–discharge cycles.

The microstructures of Fe/Fe_3O_4/N-carbon and RHC are compared in Fig. 5. The porous and hierarchical structure of the RHC matrix is clearly revealed in the secondary electron images given in Fig. 5a and b. The hierarchical structure of RHC was retained in the sample of Fe/Fe_3O_4/N-carbon as shown in Fig. 6c and d. Obviously, the iron oxide nanocomposite existed homogeneously on the porous carbon matrix in Fe/Fe_3O_4/N-carbon and Fe/Fe_3O_4/carbon. As determined by thermogravimetric analysis (TGA) (Fig. S2†), the weight of Fe/Fe_3O_4/N was increased during the thermogravimetric analysis due to the oxidation process of Fe and Fe_3O_4 to Fe_2O_3. Using the increased mass ratio of 8 wt%, the weight percentages of Fe and Fe_3O_4 are calculated as 88.5 wt% and 11.5 wt% in Fe/Fe_3O_4/N, respectively. Thus, the residual mass of Fe/Fe_3O_4/N-carbon and Fe/Fe_3O_4/carbon is 26 wt% and 30 wt%,

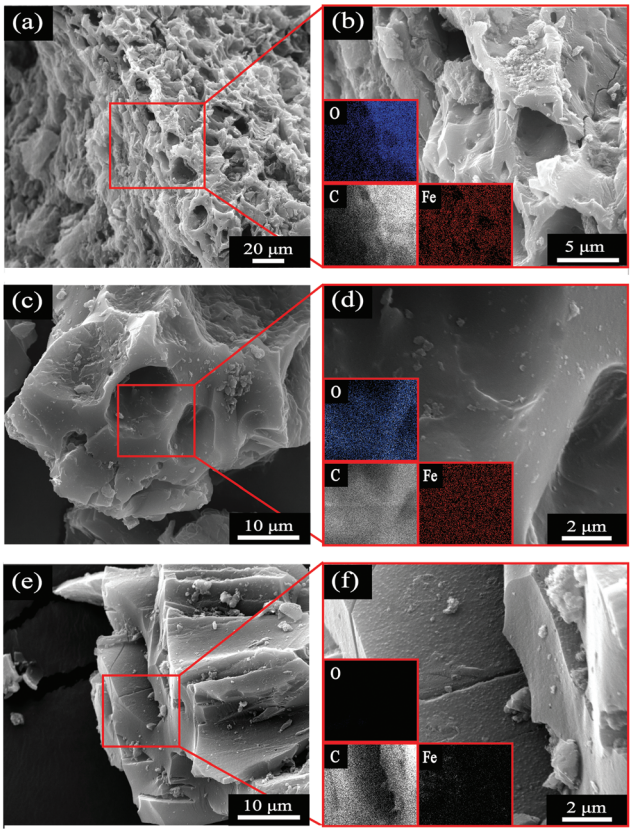

Fig. 5 SEM micrographs and mapping photograph (inset) of (a,b) Fe/Fe_3O_4/N-carbon (c,d) Fe/Fe_3O_4/carbon composite and (e,f) RHC matrix.

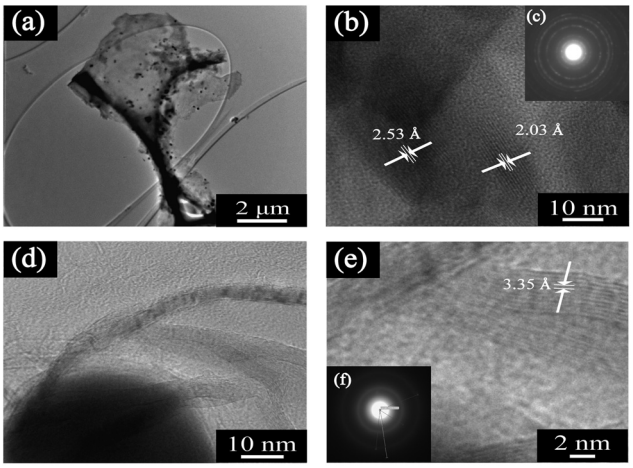

Fig. 6 TEM images and SAED pattern of the Fe/Fe_3O_4/N-carbon composite.

meaning that the carbon content in Fe/Fe_3O_4/N-carbon and Fe/Fe_3O_4/carbon is around 76 wt% and 72 wt%, respectively.

Transmission electron microscopy (TEM) images of Fe/Fe_3O_4/N-carbon are shown in Fig. 6. Particles less than 100 nm are dispersed on the RHC matrix (Fig. 6a). These nanoparticles may be either Fe_3O_4 or Fe nanoparticles in the framework formed during the calcination process, which have been con-

Published on 09 January 2015. Downloaded by University of Wollongong on 28/04/2015 02:46:58.

firmed by XRD. The average particle size is estimated to be around 47 nm (Fig. 6b), which is consistent with that of the XRD analysis. The crystal structure of Fe/Fe_3O_4 nanoparticles is revealed by the HRTEM images in Fig. 6b. The lattice spacings of 2.53 Å and 2.03 Å are ascribed to the (311) plane of Fe_3O_4 and the (110) plane of Fe, respectively. The presence of weak and large rings in the SAED pattern (Fig. 6c) for Fe/Fe_3O_4/N-carbon is evidence of the loss of sample crystallinity, in agreement with the XRD data. A randomly selected nanoparticle magnified in Fig. 6d indicated that it is wrapped with thin graphene-like layers of 5–10 nm thickness. Further investigation of these graphene-like layers found that the interplanar distance is about 0.34 nm (Fig. 6e), consisting of 5–20 graphene-like layers. The corresponding SAED pattern is also shown in Fig. 6f. The graphene-like layers were likely formed from the pyrrole vapour or other carbonaceous gasses resulting from the decomposition of rice husks with the aid of catalytic iron oxide or iron during the calcination at 800 °C. These well graphitized interconnected frameworks would provide a good electronic conductivity to the composite.

The cyclic voltammograms (CV) of the Fe/Fe_3O_4/N-carbon composite for the first two and fifth cycles in the voltage range of 3.0 to 0.01 V at a scan rate of 0.01 mV s^{-1} are shown in Fig. 7a. Two reduction peaks are observed in the first cathodic scan of Fe/Fe_3O_4/N-carbon. The peak at around 0.44 V, which is absent in the second cycle, is ascribed to the possible irreversible formation of a solid electrolyte interface (SEI) film.[29,30] The other at around 1.30 V indicates an irreversible reduction of Fe^{3+} to Fe^{2+}.[24] The anodic curves also have two peaks which are centered at about 1.59 V and 0.98 V, corresponding to the reversible oxidation of Fe^0 to Fe^{3+}or Fe^{2+}, respectively.[31,32] The peak intensity and integral areas of the fifth cycle are close to that of the second one. These results indicate that the electrochemical reversibility of Fe/Fe_3O_4/N-carbon is gradually built after the initial cycle.

The discharge/charge profiles for the first, the 2nd and the 30th cycles at 50 mA g^{-1} are given in Fig. S3.† Fe/Fe_3O_4/N-carbon shows a first-cycle insertion capacity of 748 mA h g^{-1} and a de-insertion capacity of 633 mA h g^{-1}, corresponding to a Coulombic efficiency of 85%. The second discharge and charge capacities are 594 and 545 mA h g^{-1}, respectively, with the Coulombic efficiency over 91%. Fe/Fe_3O_4/carbon shows a first-cycle insertion capacity of 647 mA h g^{-1} and a de-insertion capacity of 450 mA h g^{-1}, corresponding to a Coulombic efficiency of 70%. The second discharge and charge capacities are 517 and 440 mA h g^{-1}, respectively, with the Coulombic efficiency over 85%. The incorporation of porous carbon with a N-doped graphene-like structure significantly improves the electrochemical performance of iron oxides.

The cycling performance of Fe/Fe_3O_4/N-carbon, Fe/Fe_3O_4/carbon and RHC as anode materials for lithium ion batteries at the current density of 200 mA g^{-1} was evaluated and the results are shown in Fig. 7b. The reversible capacity of Fe/Fe_3O_4/N-carbon is ~703 mA h g^{-1} in the first cycle and then stabilizes at ~510 mA h g^{-1} after 10 cycles. Interestingly, the capacity gradually increased to ~610 mA h g^{-1} after 100 cycles. The reversible capacity of Fe/Fe_3O_4/carbon was ~647 mA h g^{-1} in the first cycle and then stabilized at ~413 mA h g^{-1} after 10

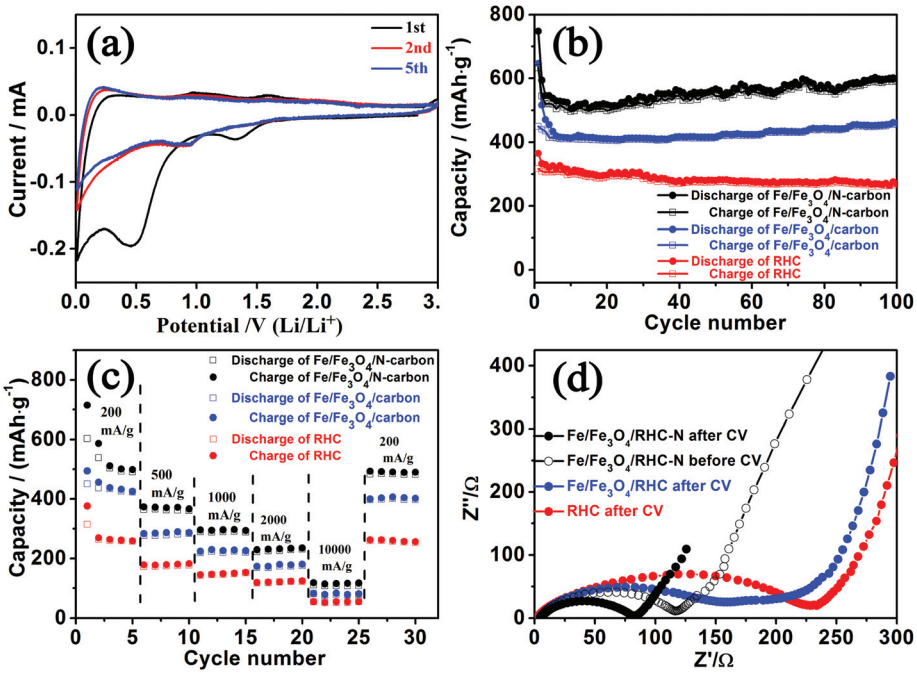

Fig. 7 (a) CV curves of Fe/Fe_3O_4/N-carbon. (b) Capacity *versus* cycle number plots of Fe/Fe_3O_4/N-carbon, RHC and Fe/Fe_3O_4/carbon in the voltage range of 0.1–3.0 V at a current density of 200 mA g^{-1}. (c) Rate capability of Fe/Fe_3O_4/N-carbon, RHC and Fe/Fe_3O_4/carbon. (d) Nyquist plots of Fe/Fe_3O_4/N-carbon, Fe/Fe_3O_4/carbon and RHC obtained by applying a sine wave with an amplitude of 5.0 mV over the frequency range from 100 kHz to 0.01 Hz.

 This journal is © The Royal Society of Chemistry 2015

Published on 09 January 2015. Downloaded by University of Wollongong on 28/04/2015 02:46:58.

cycles and then gradually increased to ~460 mA h g^{-1}. This special phenomenon of the increase in capacity with cycling can be attributed to the activating process of the porous anode as reported in Huang's work.[16] However, the porous RHC matrix did not show similar phenomenon when evaluated under the same conditions. Thus the increase of the capacity with cycling must be the consequence of the activating process of the N doping and iron oxide nanoparticles. The low reversible capacity (~260 mA h g^{-1}) of the RHC matrix under the same conditions also confirms the validity of N doping and activated nanoparticle association by facile treatment.[16,18,33,34] Among these two factors, N-doping is the main because the capacity increase is ~100 mA h g^{-1} for Fe/Fe_3O_4/N-carbon and ~47 mA h g^{-1} for Fe/Fe_3O_4/carbon.

Fig. 7c presents the rate performance of Fe/Fe_3O_4/N-carbon at current densities of 200, 500, 1000, 2000 and 10 000 mA g^{-1}, and the reversible specific capacity of 507, 301, 293, 233 and 116 mA h g^{-1} are obtained respectively. Even at a higher current density of 10 000 mA g^{-1}, the reversible specific capacity is above 116 mA h g^{-1}. The reversibility is demonstrated by the fact that a high capacity of 491 mA h g^{-1} is reached again once the rate is lowered back to 200 mA g^{-1}. However Fe/Fe_3O_4/carbon has a reversible capacity of 405 mA h g^{-1} at the current density of 200 mA g^{-1}, which is about 20% lower than that of the N-doped counterpart. A reversible capacity of 264 mA h g^{-1} for RHC has been obtained upon varying the discharge rate from 200 to 10 000 and then back to 200 mA g^{-1}. Therefore, not only the rate performance of Fe/Fe_3O_4/N-carbon is much better than that of either Fe/Fe_3O_4/carbon or RHC, but a higher capacity can be reached at a much higher rate.

The electrochemical impedance spectral (EIS) studies of Fe/Fe_3O_4/N-carbon, Fe/Fe_3O_4/carbon and RHC after 5 cycles and Fe/Fe_3O_4/N-carbon before cycles (Fig. 7d) were performed on a Chenhua CHI 660D electrochemical workstation. The Nyquist plots of Fe/Fe_3O_4/N-carbon, Fe/Fe_3O_4/carbon and RHC after 5 cycles and Fe/Fe_3O_4/N-carbon before cycles show a semicircle in the high frequency range and a sloping straight line in the low frequency range. The equivalent circuit of the electrodes is shown in Fig. S4† where the solution resistance, double layer capacitance, charge-transfer resistance and Warburg impedance are denoted asR_{el}, CPE, R_{ct}, and W, respectively. The charge-transfer resistance (R_{ct}) of the Fe/Fe_3O_4/N-carbon is calculated to be approximately 81.1 Ω after 5 cycles from 117.8 Ω, much lower than that of the Fe/Fe_3O_4/carbon and RHC electrode (approximately 162.3 and 228.6 Ω). The decreased resistance of the Fe/Fe_3O_4/N-carbon electrode is attributed to *in situ* graphene-like layers and Fe nanoparticles with excellent electrical conductivity.

The microstructure variation of Fe/Fe_3O_4/N-carbon after 100 discharge–charge cycles was examined using TEM (Fig. S5†). Obviously, no aggregation occurred and the nanoparticles are observed dispersing well after cycling. This structure observation of Fe/Fe_3O_4/N-carbon is well consistent with its cycling performance.

Consequently, the low resistance leads to the significantly enhanced rate capability of the Fe/Fe_3O_4/N-carbon composite.

It is known that the depth of lithium ion intercalation and de-intercalation in the non-graphitic carbonaceous materials strongly depends on the anode composition and structure such as crystalline phase, hydrogen content, microstructure and micromorphology.[5,35–38] As demonstrated by Zhou *et al.*[39] large and ordered pore arrays are very beneficial to the intercalation of lithium, which is known as a slow bulk-phase reaction. The hierarchical structure of our Fe/Fe_3O_4/N-carbon composite is readily accessed by the electrolyte solution, that is Li^+ ions can freely move into large pores and intercalate into the thin pore walls and the N-loading location. Therefore, the high reversibility of Li storage is probably due to the following reasons. (i) The grain size of the activated nanoparticles is less than 50 nm, which limits the anode volume change and reduces the path for Li^+ transportation. (ii) Porous carbon prevents the aggregation of activated nanoparticles. (iii) Graphene-like networks, N-doping and the generation of Fe nanoparticles increase the electronic conductivity. (iv) N-doping increases the potential Li^+ insertion locations during discharge and charge. (v) The hierarchical structure with a high surface area provides a large electrode/electrolyte contact area and a favorable pore texture for electrolyte impregnation, thus improving the anode performance. Our results clearly demonstrate that Fe/Fe_3O_4/N-carbon prepared by divertive fabrication is a promising candidate for anode materials of high reversible capacity, good cycle performance and high rate discharge/charge capability in used LIBs.

4. Conclusions

Nitrogen-doped porous carbon containing activated nanoparticles and graphene-like layers were synthesized by simple impregnation followed by polymerization and calcination methods. The resulting composite Fe/Fe_3O_4/N-carbon has a hierarchical porous structure of rice husk and contains N-doped graphene-like networks and Fe&Fe_3O_4 nanoparticles and has a high specific surface area of 1151 m^2 g^{-1}. When used as an anode in LIB, it showed a high discharge capacity of 610 mA h g^{-1} at 200 mA g^{-1} after 100 cycles and a high rate performance. Considering the abundant hierarchical structures in nature, the strategy here reported is expected to be extended for design and fabrication of other anode materials with unique structures and composition.

Acknowledgements

The authors gratefully acknowledge financial support for this research from the Morgan Crucible Company, the National Science Foundation of China (no. 51072117, 51171110), the National Basic Research Program of China (973 Program) (no. 2012CB619600), and the Shanghai Science and Technology Committee (10JC1407600, 13JC1403300, 14JC1403300, 14520710100). We also thank the Shanghai Jiao Tong University (SJTU) Instrument Analysis Center for material analyses.

Published on 09 January 2015. Downloaded by University of Wollongong on 28/04/2015 02:46:58.

Notes and references

1 J. B. Goodenough and Y. Kim, *Chem. Mater.*, 2009, **22**, 587–603.
2 V. Etacheri, R. Marom, R. Elazari, G. Salitra and D. Aurbach, *Energy Environ. Sci.*, 2011, **4**, 3243–3262.
3 S. S. Zhang, *J. Power Sources*, 2006, **162**, 1379–1394.
4 J. W. Fergus, *J. Power Sources*, 2010, **195**, 939–954.
5 Y. P. Wu, E. Rahm and R. Holze, *J. Power Sources*, 2003, **114**, 228–236.
6 L. Ji, Z. Lin, M. Alcoutlabi and X. Zhang, *Energy Environ. Sci.*, 2011, **4**, 2682–2699.
7 X. T. Chen, K. X. Wang, Y. B. Zhai, H. J. Zhang, X. Y. Wu, X. Wei and J.-S. Chen, *Dalton Trans.*, 2014, **43**, 3137–3143.
8 Y. Guo, S. Yang, K. Yu, J. Zhao, Z. Wang and H. Xu, *Mater. Chem. Phys.*, 2002, **74**, 320–323.
9 D. Kalderis, S. Bethanis, P. Paraskeva and E. Diamadopoulos, *Bioresour. Technol.*, 2008, **99**, 6809–6816.
10 T. H. Liou, *Carbon*, 2004, **42**, 785–794.
11 M. Endo, C. Kim, K. Nishimura, T. Fujino and K. Miyashita, *Carbon*, 2000, **38**, 183–197.
12 Z. Wu, W. Li, Y. Xia, P. Webley and D. Zhao, *J. Mater. Chem.*, 2012, **22**, 8835–8845.
13 Y. Li, C. Zhu, T. Lu, Z. Guo, D. Zhang, J. Ma and S. Zhu, *Carbon*, 2013, **52**, 565–573.
14 K. Xiao, Y. Liu, P. a. Hu, G. Yu, Y. Sun and D. Zhu, *J. Am. Chem. Soc.*, 2005, **127**, 8614–8617.
15 R. Czerw, M. Terrones, J. C. Charlier, X. Blase, B. Foley, R. Kamalakaran, N. Grobert, H. Terrones, D. Tekleab, P. M. Ajayan, W. Blau, M. Rühle and D. L. Carroll, *Nano Lett.*, 2001, **1**, 457–460.
16 L. Qie, W. Chen, Z. Wang, Q. Shao, X. Li, L. Yuan, X. Hu, W. Zhang and Y. Huang, *Adv. Mater.*, 2012, **24**, 2047–2050.
17 H. Wang, C. Zhang, Z. Liu, L. Wang, P. Han, H. Xu, K. Zhang, S. Dong, J. Yao and G. Cui, *J. Mater. Chem.*, 2011, **21**, 5430–5434.
18 Z. Wu, W. Ren, L. Xu, F. Li and H. Cheng, *ACS Nano*, 2011, **5**, 5463–5471.
19 X. Jin, V. V. Balasubramanian, S. T. Selvan, D. P. Sawant, M. A. Chari, G. Q. Lu and A. Vinu, *Angew. Chem., Int. Ed.*, 2009, **48**, 7884–7887.
20 M. M. Joshi, N. K. Labhsetwar, P. A. Mangrulkar, S. N. Tijare, S. P. Kamble and S. S. Rayalu, *Appl. Catal., A*, 2009, **357**, 26–33.
21 M. Lasperas, T. Llorett, L. Chaves, I. Rodriguez, A. Cauvel and D. Brunel, *Stud. Surf. Sci. Catal.*, 1997, **108**, 75–82.
22 M. A. Pimenta, G. Dresselhaus, M. S. Dresselhaus, L. G. Cancado, A. Jorio and R. Saito, *Phys. Chem. Chem. Phys.*, 2007, **9**, 1276–1290.
23 C. Thomsen and S. Reich, *Phys. Rev. Lett.*, 2000, **85**, 5214–5217.
24 L. M. Malard, M. A. Pimenta, G. Dresselhaus and M. S. Dresselhaus, *Phys. Rep.*, 2009, **473**, 51–87.
25 Y. Lin, C. Lin and P. Chiu, *Appl. Phys. Lett.*, 2010, **96**, 133110–133113.
26 A. Das, S. Pisana, B. Chakraborty, S. Piscanec, S. K. Saha, U. V. Waghmare, K. S. Novoselov, H. R. Krishnamurthy, A. K. Geim, A. C. Ferrari and A. K. Sood, *Nat. Nanotechnol.*, 2008, **3**, 210–215.
27 X. Wang, X. Li, L. Zhang, Y. Yoon, P. K. Weber, H. Wang, J. Guo and H. Dai, *Science*, 2009, **324**, 768–771.
28 J. Wang, D. N. Tafen, J. P. Lewis, Z. Hong, A. Manivannan, M. Zhi, M. Li and N. Wu, *J. Am. Chem. Soc.*, 2009, **131**, 12290–12297.
29 L. Su, Y. Zhong and Z. Zhou, *J. Mater. Chem. A*, 2013, **1**, 15158–15166.
30 C. Lei, F. Han, D. Li, W. C. Li, Q. Sun, X. Q. Zhang and A. H. Lu, *Nanoscale*, 2013, **5**, 1168–1175.
31 P. Lian, X. Zhu, H. Xiang, Z. Li, W. Yang and H. Wang, *Electrochim. Acta*, 2010, **56**, 834–840.
32 M. Ren, Z. Zhou, Y. Li, X. P. Gao and J. Yan, *J. Power Sources*, 2006, **162**, 1357–1362.
33 L. G. Bulusheva, A. V. Okotrub, A. G. Kurenya, H. Zhang, H. Zhang, X. Chen and H. Song, *Carbon*, 2011, **49**, 4013–4023.
34 F. Su, C. K. Poh, J. S. Chen, G. Xu, D. Wang, Q. Li, J. Lin and X. W. Lou, *Energy Environ. Sci.*, 2011, **4**, 717–724.
35 F. Bonino, S. Brutti, P. Reale, B. Scrosati, L. Gherghel, J. Wu and K. Müllen, *Adv. Mater.*, 2005, **17**, 743–746.
36 J. Liwen and Z. Xiangwu, *Nanotechnology*, 2009, **20**, 155705.
37 T. Zheng, Q. Zhong and J. R. Dahn, *J. Electrochem. Soc.*, 1995, **142**, L211–L214.
38 G. Zhou, D.-W. Wang, X. Shan, N. Li, F. Li and H.-M. Cheng, *J. Mater. Chem.*, 2012, **22**, 11252–11256.
39 H. Zhou, S. Zhu, M. Hibino, I. Honma and M. Ichihara, *Adv. Mater.*, 2003, **15**, 2107–2111.

This journal is © The Royal Society of Chemistry 2015